Supporting Information

Bio-Inspired Heterogeneous Sensitization of Bimetal Oxides on SnO_2 Scaffold for Unparalleled Formaldehyde Detection

Yong Jin Jeong, Dong-Ha Kim, Ji-Soo Jang, Joon-Young Kang, Rheehyun Kim, and Il-Doo Kim*

Department of Materials Science and Engineering, Korea Advanced Institute of Science and Technology (KAIST), 291 Daehak-ro, Yuseong-gu, Daejeon 34141, Korea

*Corresponding author e-mail: idkim@kaist.ac.kr

Table of Contents

Experimental details

Materials. Polyvinylpyrrolidone (PVP, M_w ~ 1,300,000 g mol^{-1}), chitosan (medium molecular weight, $(C_6H_{11}NO_4)_n$), and sodium borohydride ($NaBH_4$, ≥ 96%) were purchased from Aldrich. Nickel(II) chloride hexahydrate ($NiCl_2 \cdot 6H_2O$, ≥ 98%), tin(II) chloride dihydrate ($SnCl_2 \cdot 2H_2O$, 98%), *N,N*-dimethylformamide (DMF, 99.8%), and iron(III) chloride hexahydrate ($FeCl_3 \cdot 6H_2O$, 97%) were purchased from Sigma-Aldrich. Acetic acid (glacial, 99.8%) was purchased from SAMCHUN chemical. All materials were used without further purification.

Synthesis of SnO_2 NFs and SnO_2 FITs. We synthesized SnO_2 NFs and SnO_2 FITs as control samples. To synthesize SnO_2 NFs, we dissolved 0.35 g of PVP and 0.25 g of Sn precursor in 2 mL of DMF and stirred at 300 rpm for 5 h at room temperature. Then, we carried out electrospinning of the solution by using a feeding rate of 0.1 mL/min and a voltage of 15 kV. The distance from needle (23 gauge) to the collector was fixed at 20 cm. Subsequently, we conducted heat treatment of as-spun Sn precursor/PVP NFs at 600 ℃ for 1 h at a ramping rate of 5 ℃/min to decompose PVP and formation of SnO_2 NFs. On the other hand, SnO_2 FITs was obtained by electrospinning the solution with a reduced amount of PVP (0.3 g) and 0.25 g of Sn precursor in 2 mL of DMF, followed by subsequent calcination at 600 ℃ for 1 h.

Synthesis of NiO–SnO_2 FITs. NiO-SnO_2 FITs were synthesized as a reference sample. First, we prepared 1 w/v chitosan (CS) solution by adding 20 mg of CS in 2 mL of DI water (1% of acetic acid) and stirring the solution at 300 rpm for 12 h to completely dissolve CS at room temperature. Then, we mixed 32.4 mg of $NiCl_2 \cdot 6H_2O$ in the CS solution by stirring at 300 rpm for 2 h to form CS-Ni ions dissolved solution. Subsequenlty, 0.2 mL of separately prepared

aqueous $NaBH_4$ solution (0.1 M) was added to the CS-Ni ions dissolved solution to reduce the Ni ions to Ni nanoparticles, leading to CS-Ni^0 complex solution. Then, we incorporated 10 μL of the CS-Ni^0 complex solution into the electrospinning solution, which had the same composition as that of pristine SnO_2 FITs. Finally, electrospinning and and subsequent heat treatment were conducted to obtain NiO-SnO_2 FITs at the same conditions as for the synthesis of pristine SnO_2 FITs.

Synthesis of NiO/Fe_2O_3–SnO_2 FITs. The CS-Ni^0Fe^0 complex solution was prepared as a template for heterogeneous sensitization of NiO/Fe_2O_3 on SnO_2 FITs. First, 16.2 mg of $NiCl_2{\cdot}6H_2O$ and 19.36 mg of $FeCl_3{\cdot}6H_2O$ were dispersed in 2 mL of 1 w/v chitosan aqueous solution with 1% acetic acid. We then conducted room temperature stirring of the solution at 300 rpm for 2 h to form CS-NiFe ions solution. Subsequently, 0.2 mL of aqueous $NaBH_4$ solution (0.1 M) was added to the CS-NiFe ions solution to reduce the ions to metallic nanoparticles, resulting in the formation of CS-Ni^0Fe^0 complex solution. Then, 10, 20, 30, and 40 μL of CS-Ni^0Fe^0 complex solution were directly dispersed in separate electrospinning solutions of the same composition as that used for the synthesis of pristine SnO_2 FITs. Finally, electrospinning and subsequent calcination were carried out at the same condition as for pristine SnO_2 FITs, leading to NiO/Fe_2O_3–SnO_2 FITs with Ni/Fe wt % of 0.024, 0.048, 0.072, and 0.096.

Sensor fabrication and sensing test. We prepared alumina substrates with an area and thickness of 2.5 mm × 2.5 mm and 0.2 mm, respectively. Two parallel gold electrodes were patterned on the front side of the substrate to measure the resistance of sensing materials. In addition, the back side of the substrate was integrated with a platinum heater through which

the operating temperature was controlled. We dispersed 4 mg of each samples (SnO_2 NFs, SnO_2 FITs, NiO–SnO_2 FITs, and NiO/Fe_2O_3–SnO_2 FITs) in 0.2 mL of ethanol and then the obtained paste was drop-coated on the substrates. By using a homemade gas sensing measurement system, the sensing performance of the sensors was investigated. Prior to injection of specific gas molecules to the sensors, a fresh air (30% RH) was injected into the sensing chamber for 3 h to stabilize the base resistance of the sensors. Then, we injected the analyte gas in the concentration range of 0.2–5 ppm for 10 min, followed by a flow of fresh air for 10 min to recover the sensors to base resistances. The base resistances in air (R_{air}) and in analyte gas (R_{gas}) were converted into the response ($R = R_{air}/R_{gas}$) of the sensors. In addition, the response time was calculated as the time taken to decrease the base resistance of the sensor in air by 90% upon exposure to target gas.

Characterization. The morphologies and characteristics of the materials were confirmed by the field emission scanning electron microscopy (Nova230, FEI) and field emission transmission electron microscopy (Tecnai G2 F30 S-TWIN, FEI). To analyze the crystal structures of the samples, the high-resolution powder X-ray diffractometer (D/MAX-2500, Rigaku) with Cu Kα1 radiation (λ = 1.5418 Å) was used. The X-ray photoelectron spectroscopy (K-alpha, Thermo VG Scientific) was utilized to investigate the chemical binding states of the materials.

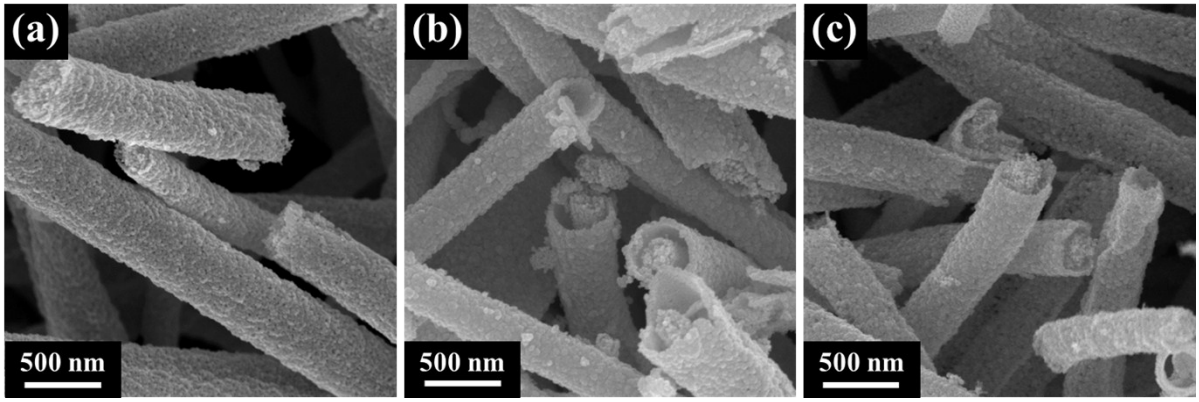

Fig. S1 SEM images of; (a) SnO_2 NFs, (b) SnO_2 FITs, and (c) NiO-SnO_2 FITs.

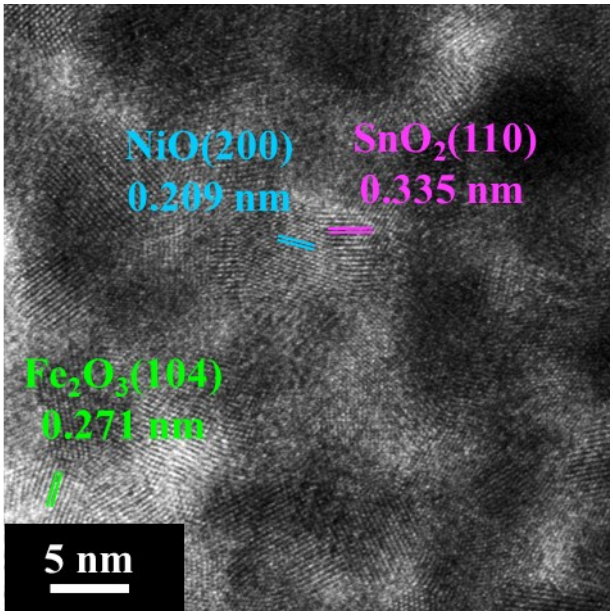

Fig. S2 HRTEM image of NiO/Fe_2O_3–SnO_2 FITs.

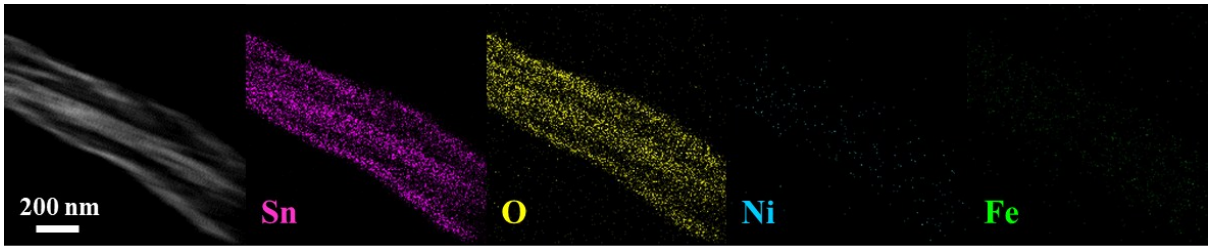

Fig. S3 EDS elemental mapping images of SnO_2 FITs

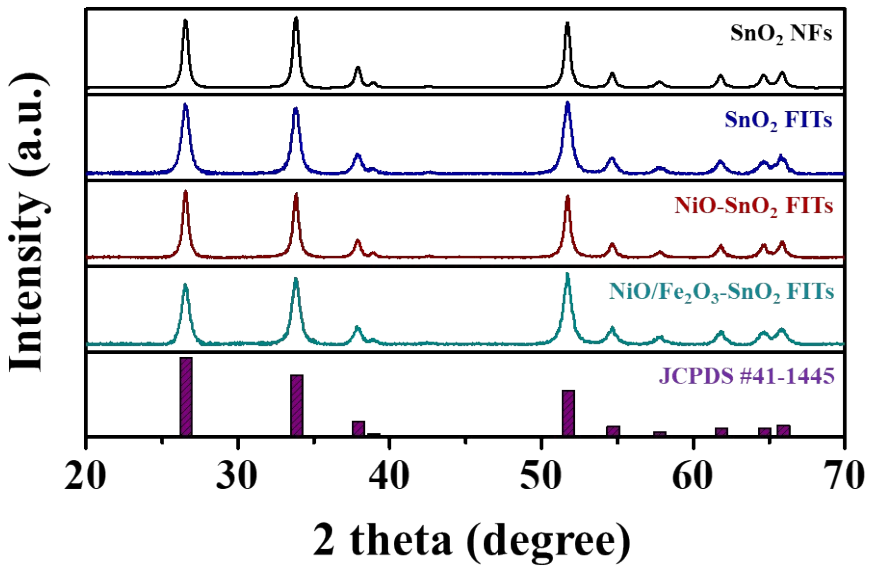

Fig. S4 XRD analysis of SnO_2 NFs, SnO_2 FITs, NiO-SnO_2 FITs, and NiO/Fe_2O_3–SnO_2 FITs.

All samples were polycrystalline rutile SnO_2 (JCPDS no. 41-1445). However, the characteristic peaks of NiO and Fe_2O_3 were not observed in the XRD analysis, and we suppose, it is due to small amounts of NiO and Fe_2O_3.

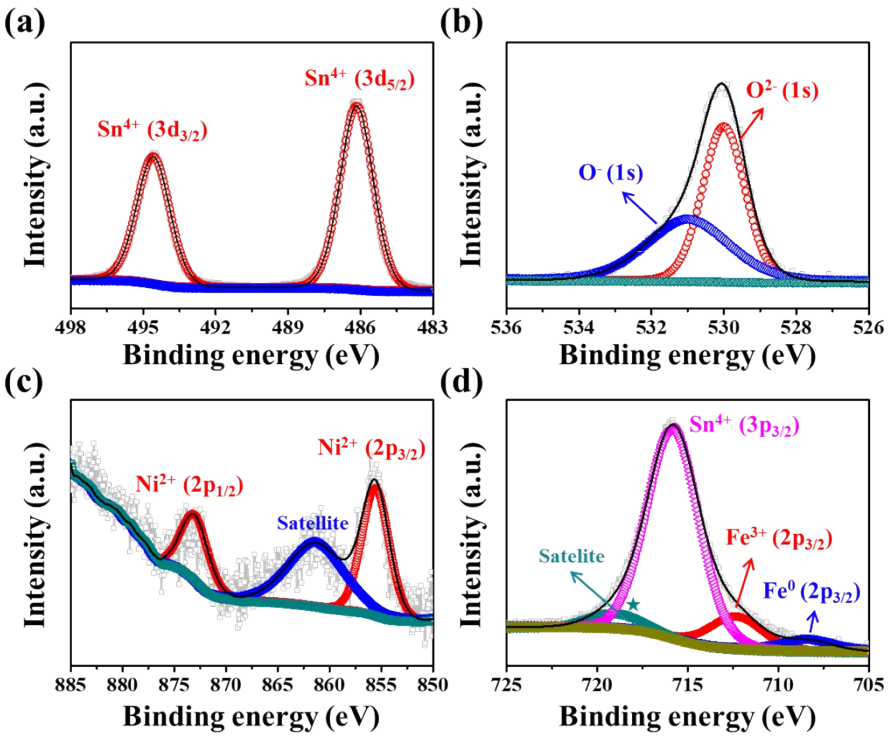

Fig. S5 XPS spectra of NiO/Fe_2O_3-SnO_2 FITs: (a) Sn 3d, (b) O 1s, (c) Ni 2p, and (d) Fe 2p.

For Sn 3d spectrum, we confirmed two obvious peaks of Sn $3d_{5/2}$ and $3d_{3/2}$, which were located at 486.2 and 494.7 eV, respectively (Fig. S5a).[1] In the case of the O 1s XPS spectrum, we identified chemisorbed oxygen (O^-) and lattice oxygen species (O^{2-}) located at 530.1 and 531.0 eV, respectively (Fig. S5b).[2] For Ni 2p XPS spectrum, two peaks were observed at 855.6 and 873.2 eV, which corresponded to Ni $2p_{3/2}$ and Ni $2p_{1/2}$ peaks of the Ni^{2+} state (Fig. S5c).[3] The Fe 2p XPS spectrum showed two peaks at 708.2 and 712.4 eV, corresponding to Fe $2p_{3/2}$ of the Fe^0 state and Fe $2p_{3/2}$ of the Fe^{3+} state, respectively (Fig. S5d), with Fe^{3+} existing as the dominant state.[4, 5] These results confirmed that Ni and Fe nanoparticles oxidized to NiO and Fe_2O_3 during calcination in air.

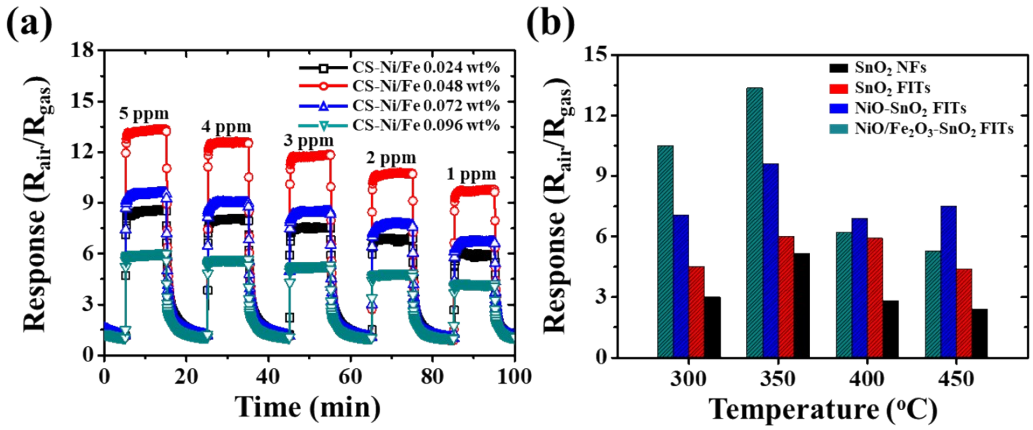

Fig. S6 (a) Dynamic formaldehyde sensing performance of NiO/Fe_2O_3-SnO_2 FITs with Ni/Fe in the range of 0.024–0.096 wt% at 350 °C. (b) Response of SnO_2 NFs, SnO_2 FITs, NiO-SnO_2 FITs, and NiO/Fe_2O_3-SnO_2 FITs toward 5 ppm of formaldehyde at different temperatures (300–450 °C).

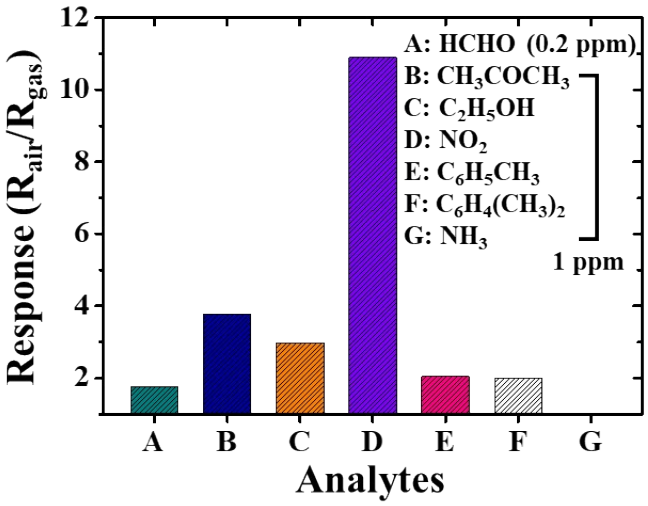

Fig. S7 HCHO selective sensing property of SnO_2 FITs against CH_3COCH_3, C_2H_5OH, NO_2, $C_6H_5CH_3$, $C_6H_4(CH_3)_2$, and NH_3.

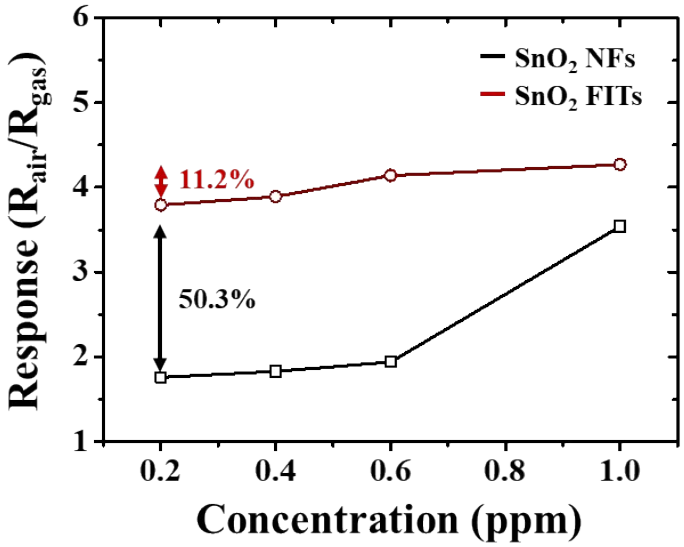

Fig. S8 Response variation of SnO_2 NFs and SnO_2 FITs in the concentration range of 0.2–1 ppm of formaldehyde gas.

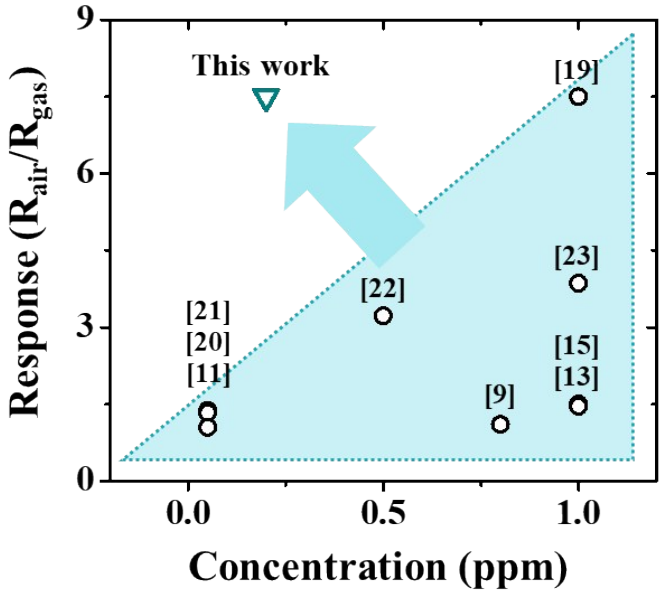

Fig. S9 0.05–1 ppm formaldehyde gas response (R_{air}/R_{gas}) of recently reported SMOs based sensors and the sensor reported in this work.

Table. S1 ICP-OES test results of NiO/Fe_2O_3–SnO_2 FITs (0.096 wt% Ni/Fe)

Test subject	Unit	Measurement results
Fe	mg/kg	586
Ni	mg/kg	268
SnO_2	%	> 99.8

Table. S2 Sensing properties of recently reported SMOs-based formaldehyde sensors.

Sensing material	Response (R_{air}/R_{gas})	Detection limit	Operating temperature	Response time	Ref.
LSCM@SnO_2 FITs	26.5 at 5 ppm	80 ppb	400 ℃	32 s at 1 ppm	6
Ag-loaded sunflower-like In_2O_3	1.5 at 5 ppm	5 ppm	240 ℃	0.9 s at 20 ppm	7
Ag@$LaFeO_3$ nanofibers	4.80 at 5 ppm	5 ppm	230 ℃	2 s at 20 ppm	8
CuO nanocubes	1.105 at 800 ppb	–	300 ℃	45 s at 800 ppb	9
CuO@TiO_2 nanofibers	15.5 at 50 ppm	5 ppm	200 ℃	1.4 s at 10 ppm	10
Pd-SnO_2 fibers	1.335 at 50 ppb	50 ppb	140 ℃	53 s at 100 ppb	11
WO_x@In_2O_3 nanosheets	25 at 100 ppm	0.1 ppm	170 ℃	1 s at 100 ppm	12
In_2O_3 nanoparticle-flowerlike ZnO	1.5 at 1 ppm	1 ppm	240 ℃	1.5 s at 50 ppm	13
Hierarchical ZnO architectures	35 at 100 ppm	–	260 ℃	1 s at 100 ppm	14
α-Fe_2O_3@NiO core-shell nanofibers	1.46 at 1 ppm	< 1 ppm	240 ℃	2 s at 50 ppm	15
Ce@Sn_3O_4 hierarchical microspheres	5.50 at 100 ppm	–	200 ℃	4 s at 200 ppm	16
SnO_2 microtubes	26.2 at 100 ppm	10 ppb	92 ℃	4–200 s at 1–100 ppm	17
SnO_2 microspheres	38.28 at 100 ppm	–	200 ℃	17 s at 100 ppm	18
Co-rich $ZnCo_2O_4$ hollow nanospheres	7.5 at 1 ppm	13 ppb	230 ℃	149 s at 1 ppm	19
Single-crystalline Co_3O_4 nanoparticles	1.05 at 50 ppb	50 ppb	220 ℃	75 s at 3 ppm	20
Hierarchical flower-like CuO nanostructure	1.378 at 50 ppb	50 ppb	250 ℃	–	21
NiO nanoroses	3.22 at 500 ppb	50 ppb	230 ℃	58.5 s at 500 ppb	22
Hierarchical porous SnO_2 micro-rods	3.86 at 1 ppm	50 ppb	330 ℃	4.3 s at 1 ppm	23
NiO/Fe_2O_3-SnO_2 FITs	7.44 at 200 ppb	< 5 ppb	350 ℃	12 s at 200 ppb	this work

References

1 Y. Cui, G. Wang and D. Pan, *CrystEngComm*, 2013, **15**, 10459–10463.

2 J. S. Jang, Y. W. Lim, D. H. Kim, D. Lee, W. T. Koo, H. Lee, B. S. Bae and I. D. Kim, *Small*, 2018, 1802260.

3 W. Lu, X. Qin, A. M. Asiri, A. O. Al-Youbi and X. Sun, *Analyst*, 2013, **138**, 429–433.

4 H. Lv, H. Zhao, T. Cao, L. Qian, Y. Wang and G. Zhao, *J. Mol. Catal. A: Chem.*, 2015, **400**, 81–89.

5 R. Liang, L. Shen, F. Jing, N. Qin and L. Wu, *ACS Appl. Mater. Interfaces*, 2015, **7**, 9507–9515.

6 J.-Y. Kang, J.-S. Jang, W.-T. Koo, J. Seo, Y. Choi, M.-H. Kim, D.-H. Kim, H.-J. Cho, W. Jung and I.-D. Kim, *J. Mater. Chem. A*, 2018, **6**, 10543–10551.

7 S. Wang, B. Xiao, T. Yang, P. Wang, C. Xiao, Z. Li, R. Zhao and M. Zhang, *J. Mater. Chem. A,* 2014, **2**, 6598–6604.

8 W. Wei, S. Guo, C. Chen, L. Sun, Y. Chen, W. Guo and S. Ruan, *J. Alloys Compd.*, 2017, **695**, 1122–1127.

9 H. J. Park, N.-J. Choi, H. Kang, M. Y. Jung, J. W. Park, K. H. Park and D.-S. Lee, *Sens. Actuators, B*, 2014, **203**, 282–288.

10 J. Deng, L. Wang, Z. Lou and T. Zhang, *J. Mater. Chem. A*, 2014, **2**, 9030–9034.

11 S. Tian, X. Ding, D. Zeng, J. Wu, S. Zhang and C. Xie, *RSC Adv.*, 2013, **3**, 11823–11831.

12 Y. Cao, Y. He, X. Zou and G.-D. Li, *Sens. Actuators, B*, 2017, **252**, 232–238.

13 S. Wang, Z. Li, P. Wang, C. Xiao, R. Zhao, B. Xiao, T. Yang and M. Zhang, *CrystEngComm*, 2014, **16**, 5716–5723.

14 J. Cao, S. Wang and H. Zhang, *Mater. Lett.*, 2017, **202**, 44–47.

15 J. Cao, Z. Wang, R. Wang, S. Liu, T. Fei, L. Wang and T. Zhang, *J. Mater. Chem. A*, 2015, **3**, 5635–5641.

16 X. Ma, J. Shen, D. Hu, L. Sun, Y. Chen, M. Liu, C. Li and S. Ruan, *J. Alloys Compd.*, 2017, **726**, 1092–1100.

17 W. Zhang, X. Cheng, X. Zhang, Y. Xu, S. Gao, H. Zhao and L. Huo, *Sens. Actuators, B*, 2017, **247**, 664–672.

18 Y. Li, N. Chen, D. Deng, X. Xing, X. Xiao and Y. Wang, *Sens. Actuators, B*, 2017, **238**, 264–273.

19 H. J. Park, J. Kim, N.-J. Choi, H. Song and D.-S. Lee, *ACS Appl. Mater. Interfaces*, 2016, **8**, 3233–3240.

20 J. Y. Kim, N.-J. Choi, H. J. Park, J. Kim, D.-S. Lee and H. Song, *J. Phys. Chem. C*, 2014, **118**, 25994–26002.

21 H. Deng, H.-r. Li, F. Wang, C.-x. Yuan, S. Liu, P. Wang, L.-z. Xie, Y.-z. Sun and F.-z. Chang, *J. Mater. Sci.: Mater. Electron.*, 2016, **27**, 6766–6772.

22 Y. Zhang, L.-Z. Xie, C.-X. Yuan, C.-L. Zhang, S. Liu, Y.-Q. Peng, H.-R. Li and M. Zhang, *Nano*, 2016, **11**, 1650009.

23 K. Xu, D. Zeng, S. Tian, S. Zhang and C. Xie, *Sens. Actuators, B*, 2014, **190**, 585–592.